BNL-43559
OG-1094

Subm. to 1989 IEEE Nucl. Sci. Symp., San Francisco, CA

Readout Techniques and Radiation Damage of Undoped Cesium Iodide

C.L.Woody, P.W.Levy, J.A.Kierstead
Brookhaven National Laboratory
Upton, New York 11973

T.Skwarnicki, Z.Sobolewski, M.Goldberg, N.Horwitz, P.Souder
Physics Department, Syracuse University
Syracuse, New York 13244

D.F.Anderson
Fermi National Accelerator Laboratory
Batavia, Illinois 60510

ABSTRACT

Several readout techniques for undoped CsI have been studied which utilise the fast scintillation component for speed, and the high photon yield for good energy resolution. Quantum yields have been measured for samples up to 30 cm in length using photomultiplier tubes, wavelength shifters, and silicon photodiodes. A study has also been made of the scintillation properties of undoped CsI. It is found that the light output and decay time of the 310 nm fast component increases and the emission spectrum shifts to longer wavelengths at lower temperatures. The effects on the optical transmission and scintillation light output due to radiation damage from ^{60}Co gamma rays has been measured for doses up to $\sim 10^6$ rad. It is found that the radiation resistance of undoped CsI is substantially higher than has been reported for thallium doped CsI.

1. INTRODUCTION

It has recently been reported that undoped cesium iodide (CsI) exhibits a fast scintillation emission at $\sim$ 310 nm which can be characterised by two decay times, $\tau_1 \sim 10$ ns and $\tau_2 \sim 35$ ns [1]. This emission was observed many years ago in the study of the luminescence of thallium doped cesium iodide (CsI(Tl)) [2]. In addition to this fast component, there is also a slow component with a decay time of several microseconds which appears to be partly related to impurities in the crystal [3]. The fast scintillation properties and high density (4.5 gm/cm^3) make CsI an attractive material for use as a high resolution electromagnetic calorimeter at high rates, as well as for positron emission tomography. In addition, undoped CsI is produced using a technology similar to that used for CsI(Tl) which has been produced in multi-ton quantities [4]. Undoped CsI therefore offers promising possibilities for large, high rate detectors for high energy and nuclear physics, as well as for medical imaging.

This paper discusses some of the basic properties of undoped CsI and describes several techniques for reading out the fast component. These include photomultiplier tubes (PMT) coupled directly to the crystal, wavelength shifters read out with PMT's, and silicon photodiodes. In the case of the PMT and wavelength shifter readout, the quantum yields have been determined separately for the fast and slow components. The change in the intensity, decay time and emission spectrum of the scintillation light output is also discussed. Finally, results are given on the loss of transmission and light output due to radiation damage from ^{60}Co gamma rays.

2. READOUT TECHNIQUES

Direct PMT

The simplest type of readout for undoped CsI is to couple the crystal directly to a quarts or uv glass window PMT. This method gives the greatest photoelectron yield combined with high gain and low noise, and is therefore the best technique for measuring energies in the few MeV range. It is also possible to obtain excellent energy resolution at higher energies ($\sigma/mean \sim 2\%/\sqrt{E}$ at ~ 1 GeV) with this method [5].

Table I

Photoelectron Yield and Energy Resolution of Large Undoped CsI Crystals

Supplier	Size(cm)	Short Gate (100 ns) Npe/MeV	ΔE/E	Long Gate (1μs) Npe/MeV	ΔE/E	S/L Ratio
Horiba	5x5x15	199 ± 5	.25 ± .01	292 ± 5	.24 ± .01	.66
Horiba	6.1x30	129 ± 5	.27 ± .01	159 ± 5	.27 ± .01	.81
Bicron	5x5x15	262 ± 5	.19 ± .01	351 ± 5	.18 ± .01	.75
Bicron	6.1x30	175 ± 5	.27 ± .01	225 ± 5	.28 ± .01	.78
BDH	5x5x20	203 ± 5	.21 ± .01	250 ± 5	.21 ± .01	.81
BDH A	6.1x30	50 ± 5	.37 ± .01	77 ± 5	.35 ± .01	.64
BDH B	6.1x30	102 ± 5	.35 ± .01	154 ± 5	.32 ± .01	.66
Harshaw	5x5x15	140 ± 5	.25 ± .01	213 ± 5	.23 ± .01	.66

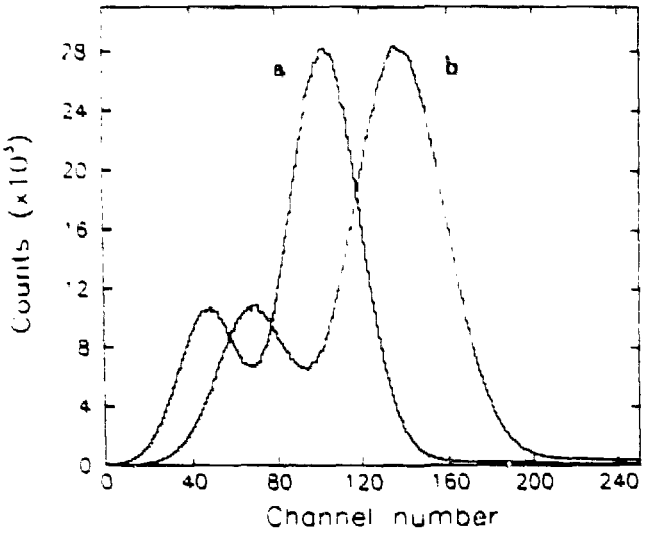

Fig. 1: Pulse height distributions for the Bicron hexagon for ^{137}Cs a) 100 ns gate b) 1 μs gate.

The photoelectron yields for a number of large crystals was measured using a quarts window PMT (Hamamatsu R2059) and are given in Table I. Each crystal was wrapped with two layers of white reflecting teflon tape and coupled directly to the tube with a uv transmitting silicon fluid (GE Viscasil 600M). The number of photoelectrons produced per unit energy deposit in the crystal was determined from the photopeak of the pulse height distribution from a ^{137}Cs source ($E_\gamma = 662KeV$) and an independent determination of the single photoelectron pulse height from the PMT. Measurements were made with a LeCroy 3001 qVt using integration times (gate lengths) of 100 ns and 1 μs. Also given are the energy resolutions $\Delta E\,(fwhm)\,/E$ obtained at 662 KeV and the ratio of photoelectrons measured for the short and long gates.

The samples ranged in size from 15 cm in length with a 5x5 cm square cross section to 30 cm in length with a 6.1 cm flat-to-flat hexagonal cross section. The best of the large hexagonal crystals was obtained from Bicron and gave 175 pe/Mev for the short gate and 225 pe/MeV for the long gate, with a ratio of short/long (S/L) of 0.78. The pulse height spectra for ^{137}Cs obtained with this crystal for the short and long gates are shown in Fig. 1.

Overall, the photoelectron yields and energy resolutions for the large crystals are quite good. There is, however, a large sample to sample variation, especially from manufacturer to manufacturer. Also, 2-3 times higher photoelectron yields and S/L ratios $\gtrsim 0.9$ have been observed in smaller samples (e.g., 2.54 cm dia. x 2.54 cm long cylinders), indicating that it is in principle possible to obtain higher quality material. Table I also shows that that the resolutions are in general poorer than that due to photoelectron statistics alone, implying that there other factors contributing to the observed resolution in larger crystals.

It is worth noting that the photoelectron yields for the fast component in CsI are roughly a factor of two higher than for the fast component of BaF_2 crystals of comparable size [6]. Moreover, taking the S/L ratio as a measure of the ratio of fast to slow component in the crystal, this ratio is much higher in undoped CsI than in BaF_2 (~ 0.8 for the best large CsI crystals compared with $\lesssim 0.2$ for BaF_2). Therefore, although the fast component in CsI is not as fast as in BaF_2, the slow component is considerably less intense and will cause less pileup at high rates.

Figure 2 shows the detected fast component light output of the Bicron hexagon for various source positions along the length of the crystal. The solid points are for the PMT coupled to one end of the crystal and the open points are for the PMT coupled to the other end. The light output is nearly constant in the first orientation, while in the second orientation, approximately 15% less light is detected from the end farthest from the readout. This implies that there is a nonuniformity in the light output within the crystal, which can be compensated for by orienting the end with the highest light output away from the PMT. The data also imply that the effective attenuation length in this sample is quite long. However, the effective attenuation length reflects the actual absorption length in the material (typically $\gtrsim 60$ cm) and the light collection efficiency for a particular geometry. It is therefore not necessarily indicative of

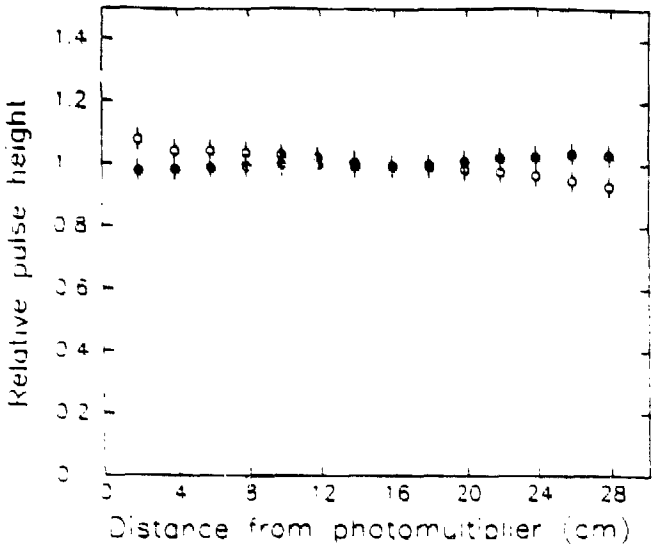

Fig. 2: Fast component light output measured for various source positions along the length of the Bicron hexagon. Solid circles - first orientation; Open circles - second orientation (see text).

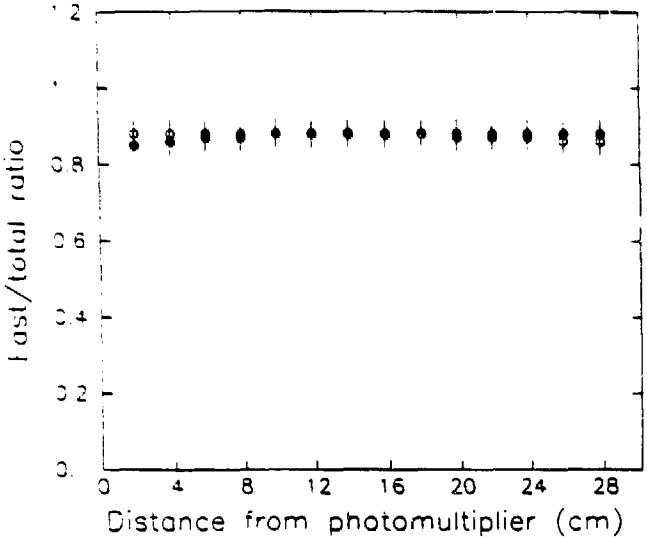

Fig. 3: Fast/total (S/L) ratio measured for various source positions along the length of the Bicron hexagon. Solid circles - first orientation; Open circles - second orientation (see text).

what the effective attenuation length would be for other geometries.

Fig. 3 shows the S/L ratio measured along the same crystal. The ratio is approximately flat for both orientations, indicating that ratio of the fast to slow component is nearly constant across the length. Similar results for both the fast component light output and S/L ratio were observed with other large samples.

There has been some evidence in the literature that the slow component in CsI is emitted at much longer wavelengths ($\gtrsim$ 400 nm) than the fast component [1]. If

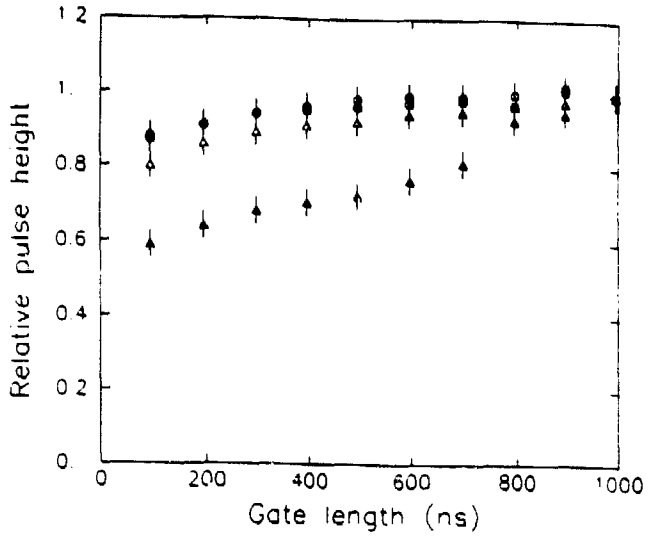

Fig. 4: Relative pulse height vs gate length: Solid circles - Harshaw crystal, no filter; Open circles - Harshaw crystal, with filter; Solid traingles - Bicron crystal, no filter; Open triangles - Bicron crystal, with filter.

this were true, it should be possible to reduce the slow component detected in the readout by interposing an optical filter between the crystal and PMT which passes the 310 nm light and suppresses all other wavelengths.

The slow component suppression using this technique was measured with a broad band pass filter (Oriel No. 51800) with a peak transmission of 96% at 320 nm and 20%(0.2%) at 400(425) nm. Figure 4 gives the fraction of light collected as a function of integration time for two undoped CsI crystals with and without the filter. In each case, the fraction is normalised to 1.0 at 1 μs. The samples tested were 2.54 cm dia. x 2.54 cm long cylinders. The fraction of light collected for 100 ns is equivalent to the S/L ratio, while the rest of the curve gives the amount of light collected for longer times. The open points show the Harshaw (now Engelhart, Inc.) crystal with and without the filter. This crystal, which had a good intrinsic S/L ratio ($\sim$ .85), did not improve with the filter. The other sample, from Bicron, had a poor intrinsic S/L ratio ($\sim$ .59) and improved significantly to $\sim$ 0.8 with the filter. Other samples with poor intrinsic S/L ratios showed similar increases, but in no case did the S/L ratio increase beyond $\sim$ 0.9 with the filter. This would imply only part of the slow component emission spectrum is cut out by the filter. However, part of the slow emission must occur at wavelengths shorter than 400 nm which makes it difficult to separate spectrally from the fast component. This may also indicate that some of the slow component is not related to impurities in the crystal.

Wavelength shifters

Another readout possibility for undoped CsI is to use the uv scintillation light to excite a wavelength shifter

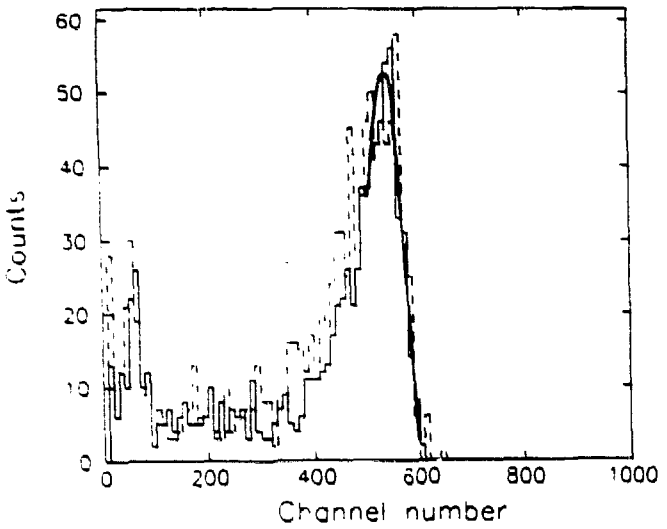

Fig. 5: Pulse height distribution for 3 GeV electrons in the Horiba hexagon with direct readout (solid histogram) and BC 408 wavelength shifter readout (dashed histogram). The curve indicates the region which was fit to obtain the resolution.

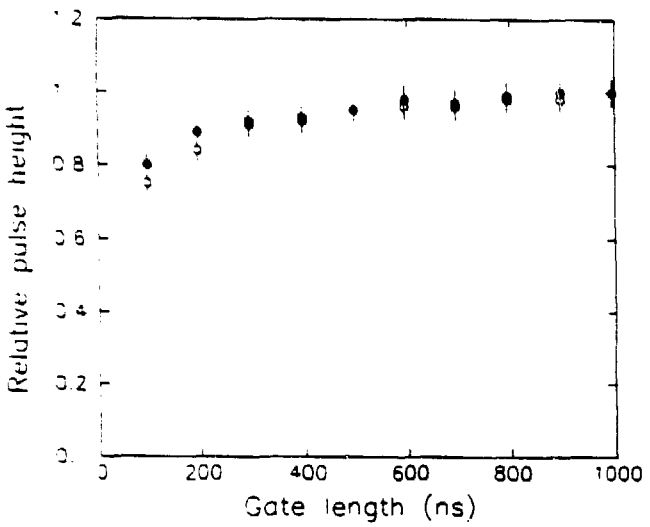

Fig. 6: Relative pulse height vs. gate length for the Horiba hexagon: Solid points - direct readout; Open points - BC 408 wavelength shifter readout.

of the type used in plastic scintillators. This shifts the primary uv light to longer wavelengths where many photon detectors are more sensitive and eliminates the need for quarts windows. It also allows the possibility of reading out many crystals with a single wavelength shifter the same way that multiple layers of scintillator plates are read out with a wavelength shifting bar in a sampling calorimeter. This could be used, for example, to read out an array of crystals with a single wavelength shifter with PMT's on each end. The difference in pulse height and timing from the two tubes could be used to determine the location of the shower along the length of the array.

The wavelength shifting readout technique was studied using the Horiba hexagon with several types of wavelength shifters. A wavelength shifter measuring 7.7x4.9 cm^2 by 0.9 cm thick was placed $\sim$ 0.5 mm from the readout end of the crystal. It was wrapped with aluminum foil on all sides except the surface facing the crystal and was read out on one 4.9x0.9 cm^2 end with a glass window PMT (Hamamatsu R1828-02). With this arrangement, the PMT did not view any direct light coming from the crystal.

The highest photoelectron yield was obtained with a piece of Bicron BC 408 scintillator used as the wavelength shifter. This gave a value of 44 p.e./MeV for the short gate and 56 p.e./MeV for the long. The number of photoelectrons per MeV obtained with the wavelength shifter was $\sim$ 25% of the number detected directly with a quarts window PMT for both the long and short gates. Another wavelength shifter, consisting of BC 408 flours embedded in acrylic, gave $\sim$ 15%. It is not clear why the acrylic sample gave a lower value.

This same arrangement was used to study the response of a large crystal to high energy showers. Figure 5 shows the pulse height distribution obtained with the Horiba hexagon for 3 GeV electrons in a test beam at the Brookhaven AGS. The solid histogram gives the distribution for the direct readout with the quarts window PMT and the dashed histogram gives the distribution for the wavelength shifter readout using the BC 408 scintillator shifter and glass window PMT. The gains were adjusted such that the electron peak occurred in approximately the same channel in both cases. Since the crystal did not provide sufficient containment at this energy, the resolution is dominated by transverse and longitudinal leakage. Nevertheless, a resolution of $\sigma/mean \sim 4\%$ was obtained by applying a Gaussian fit to the upper part of the curves as shown in the figure. This indicates that, at least at high energies, it is possible to obtain a resolution with the wavelength shifter which is comparable to the direct readout.

Since the wavelength shifter is primarily excited by the 310 nm fast component, any slow emission at longer wavelengths should be suppressed since the PMT does not view any direct light coming from the crystal. One would therefore expect that if the slow emission occurs mainly at longer wavelengths, the S/L ratio for a given crystal should improve with the wavelength shifter readout. We find however that this is not the case. Figure 6 shows the fraction of light collected as a function of integration time for the Horiba hexagon for the direct and wavelength shifter readout. Since there is very little difference between the two, we again conclude that part of the slow emission occurs at shorter wavelengths, similar to the fast component.

Silicon photodiodes

Silicon photodiodes offer another possibility for reading out undoped CsI. Devices currently available have good

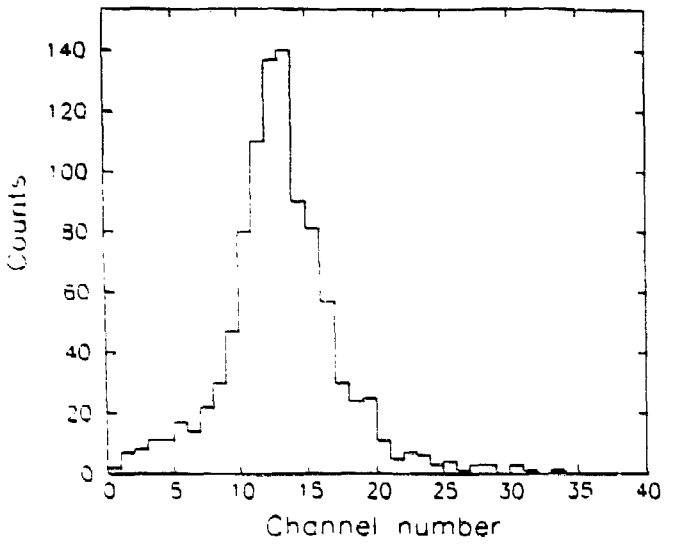

Fig. 7: Pulse height distribution for cosmic rays for the 5x5x20 cm^3 BDH crystal with silicon photodiode readout.

Table II

Photoelectron Yields For Silicon Photodiode Readout

Sample size (cm)	$E_{dep}(MeV)$	Npe/MeV
1.27 x 1.27 x 2.54	7	680
2.54 dia. x 2.54	14	540
5 x 5 x 20	110	117

quantum efficiencies ($\gtrsim$ 30%) in the 300 nm wavelength range and have rise times $\sim$ 10 ns, which is well matched to the decay time of the fast component in the crystal. This type of readout could be used inside a magnetic field and is an attractive possibility for reading out large, highly segmented arrays of crystals.

A previous result reported a light yield of 16,800 photons per MeV for undoped CsI based on a measurements with silicon photodiodes [7]. This implies an intrinsic light output $\sim$ 40% of NaI, which is in gross disagreement with the value of 4% claimed by the group that discovered the fast scintillation component in undoped CsI [3]. However, the samples measured in ref. [7] were of questionable purity, which may explain their unusually high light yield.

The photoelectron yields have been measured for several undoped CsI crystals coupled directly to a Hamamatsu S-3590-03 silicon photodiode. The samples were polished on all surfaces and completely wrapped except for the readout area with white reflecting teflon tape. The crystal was coupled to the photodiode with uv transmitting silicon fluid. Cosmic rays were used as a source of energy deposit in the crystals. A set of small scintillation counters above and below the samples were used to define the cosmic ray trigger. The cosmic rays selected by the trigger did not pass through the active area of the photodiode. The photodiode was connected to a preamplifier of the type used by the CLEO II collaboration [8] and was followed by a shaping amplifier with a shaping time of 2 μs. In this configruation, the noise observed was $\sim$ 700 electrons rms. The noise increased to $\sim$ 800 electrons rms with a shaping time of 0.5 μs with no significant change in the photoelectron yields. It would clearly be interesting to use shorter shaping times in order to take full advantage of the speed of the crystal, but this was not possible with our present electronics.

Figure 7 shows the pulse height distribution for cosmic rays obtained with a the 5x5x20 cm^3 BDH sample. The average energy deposit was $\sim$ 110 MeV and the observed distribution had a $fwhm/mean \sim 45\%$. Table II gives the photoelectron yields measured for three different samples along with the average energy deposit in each crystal. For comparison, the photoelectron electron yield for the large crystal measured with the PMT is given in Table I, and is 296 (573) pe/MeV for the 1.27x1.27 cm^3 (2.54 cm dia.) samples. There is clearly a strong dependence of the photoelectron yield on the size of the crystal. The photodiode active area is only 1x1 cm^3 and therefore does not cover the entire readout area of even the smallest crystal. The photoelectron yield is largely determined by the light collection factor which is lowest for the large crystal. In this case, the photoelectron yield could be improved by covering the readout area with more than one photodiode, but the signal to noise ratio for each would remain the same. For the large crystal, this would correspond to a useful low energy threshold ($\sim 5\sigma_{noise}$) of $\sim$ 32 MeV. The same threshold for the smallest crystal would be $\sim$ 5 MeV.

A similar measurement was made with two CsI(Tl) samples, one 1x1x2.54 cm^3 and the other 2.54x2.54x2.54 cm^3. In this case, the photodiode was a Hamamatsu S-1723-06 connected to the same readout electronics but with a factor of 30 less gain. The rms noise was again $\sim$ 700 electrons. The photoelectron yields measured for the two samples were 23,900 p.e./MeV and 15,800 p.e./MeV respectively. It is difficult to determine the absolute photon yields for each crystal due to the different geometries and hence different light collection efficiencies. However, after correcting for the quantum efficiencies of the photodiodes at the different peak emission wavelengths of undoped CsI and CsI(Tl), a ratio is obtainied for the intrinsic light output of undoped CsI relative to CsI(Tl) of approximately 6-7 %, where the range covers the uncertainty in the light collection efficiencies. This agrees well with a value of 6% we measured with similar crystals using a PMT, and is also consistent with the value of 4% for the ratio of undoped CsI to NaI reported in ref. [3].

3. TEMPERATURE DEPENDENCE

It was reported in ref. [3] that the light output of undoped CsI has a temperature coefficient $\sim$ -1.5%/^oC near room temperature. This is similar to the temperature

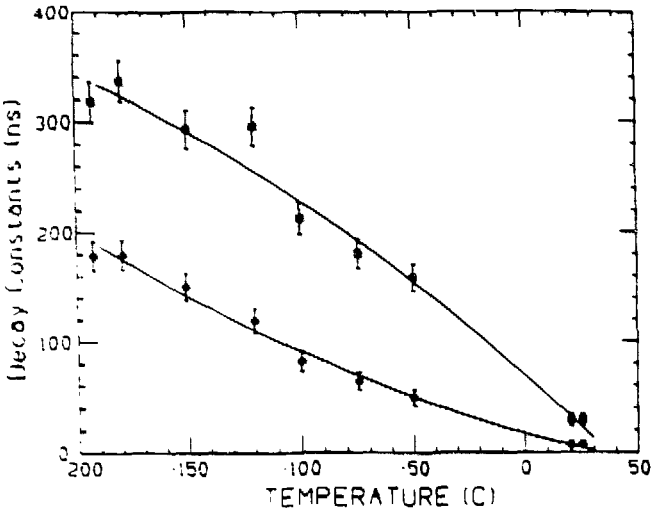

Fig. 8: Variation in the decay constants of the fast components in undoped CsI as a function of temperature.

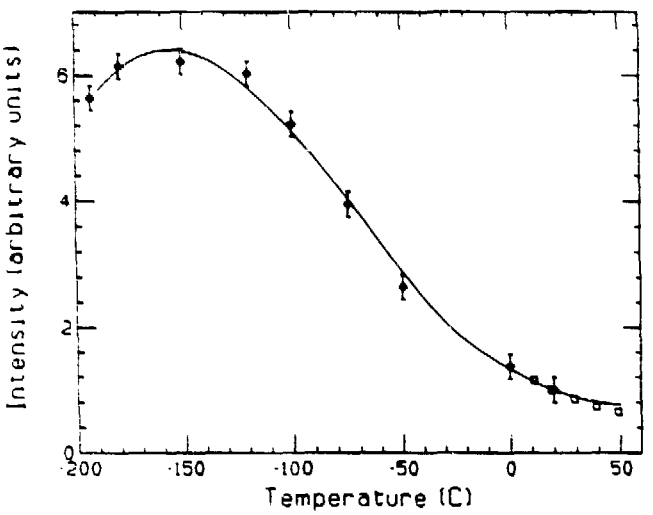

Fig. 9: Variation in the light output of the sum of both fast components in undoped CsI as a function of temperature.

coefficient observed in other crystals such as BGO [9] and the slow component in BaF_2 [10].

To study the temperature dependence of undoped CsI, a 1x1x1 cm^3 crystal was placed in a liquid nitrogen cryostat and viewed through a quarts window by a PMT kept at room temperature. A ^{22}Na source was used to excite the sample and simultaneously produce a signal a small BaF_2 crystal read out with a second PMT. The BaF_2 signal was used to start a time to digital converter and the signal from the CsI was used as a stop. The distribution of stop pulses was used to obtain the intensity and decay time of the CsI light output. Additional details regarding this technique can be found in ref. [11].

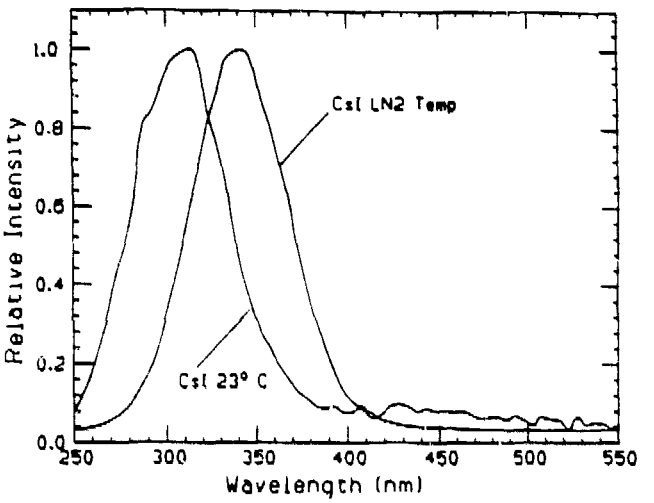

Fig. 10: Emission spectrum of undoped CsI at 23°C and liquid nitrogen temperature.

The change in the decay times of the fast components as a function of temperature are shown in Figure 8. These components, which are characterised by two decay times, $\tau_1 \sim 7$ ns and $\tau_2 \sim 29$ ns at room temperature (in rough agreement with 10 ns and 35 ns reported in [3]), increases to $\sim$ 180 ns and $\sim$ 320 ns, respectively, at $\sim -190°C$. The total intensity, including both fast components, as a function of temperature is shown in Figure 9. The intensity increases by approximately a factor of 6 at $\sim -150°C$ and decreases slightly at lower temperatures.

This result is very different than the temperature behavior of BaF_2. The fast emission in BaF_2 is thought to be due to a so-called crossover transition [12] and exhibits no variation with temperature over a fairly large range [10]. This indicates that the fast scintillation mechanism in undoped CsI is fundamentally different than in BaF_2. However, the effect of increased light intensity and longer decay times at lower temperatures have been observed in other scintillators such as CdF_2 [13] and BGO [9].

The increased light yield at low temperature was also confirmed by a measurement with the silicon photodiode. The 1.27x1.27x2.54 cm^3 crystal and photodiode were cooled to liquid nitrogen temperature and excited with a ^{137}Cs source. A clear photopeak was observed which corresponded to $\sim$ 9900 pe/MeV, compared with 680 pe/MeV at room temperature. This is a factor of 14.6 increase, compared with the factor of 6 observed with the PMT. However, it has been reported that the emission specturum of undoped CsI shifts to longer wavelengths at lower temperatures [2]. Since the quantum efficiency of the photodiode is higher at longer wavelengths, this could explain part of the increase in the observed photoelectron yield.

The shift in the emission spectrum at low temperature was confirmed by our own measurements. Figure 10

shows the emission spectrum for undoped CsI at room and liquid nitrogen temperature. There is a shift in the peak emission from 310 nm to 340 nm at the lower temperatures. This would produce only a $\sim$ 3% increase in photoelectron yield due to quantum efficiency of the photodiode. The difference between the increase observed with the photodiode and the PMT could be due to a difference between the two samples or a change in the photodiode characteristics at lower temperatures.

4. RADIATION DAMAGE

Radiation damage in scintillating materials can severly limit their usefulness in certain applications. This damage is caused by the formation of color centers that reduce the light transmission, or by destroying the luminescent centers in the material. It has been shown that CsI(Tl) is suseptible to radiation damage at rather low doses ($\lesssim 10^3$ rad) [14]. However, it would not be suprising if undoped CsI were considerably more radiation resistant than CsI(Tl) due to the fact that radiation induced color center formation is largely dependent on the presence of impurities in the crystal lattice.

A total of five undoped CsI samples 2.54 cm dia. x 2.54 cm long were irradiated with gamma rays to doses in excess of 10^6 rad at the ^{60}Co Radiation Facility at Brookhaven National Lab [15]. The samples were irradiated in a atmospherically controlled chamber through which dry nitrogen flowed continuously to prevent any surface deterioration due to moisture during the exposure. The optical transmission and scintillation light output were measured before and after irradiation to determine separately the loss in light output due to increased absorption and reduced scintillation in the material. In addition, the radiation source was temporarily removed at periodic intervals during the exposure in order to measure the transmission through the samples. These measurements were made typically within 3-5 minutes after removing the source to observe any effects of radiation damage which have a short recovery time.

Figure 11 shows the radiation induced absorption for two samples, one from Horiba and another from Bicron. These samples were typical of the other samples measured. The data are given in terms of the induced absorption coefficient α as a function of wavelength, where α is defined as $I = I_o e^{-\alpha s}$, and s is the sample thickness in cm. The induced absorption is defined as the increase in absorption relative to the unirradiated sample. The solid curves shown are for doses of 10^3, 10^4, 10^5, 10^6 and 1.5×10^6 rad in order of increasing absorption. The squares show the absorption measured 3 days after the radiation was halted. During the recovery period, the samples were kept in the dark at room temperature.

Both samples show a prominent absorption band at $\sim$ 800 nm and several bands in the 250-550 nm region. This 800 nm band has been observed before and has been tentatively identified as due to an F-center [16].

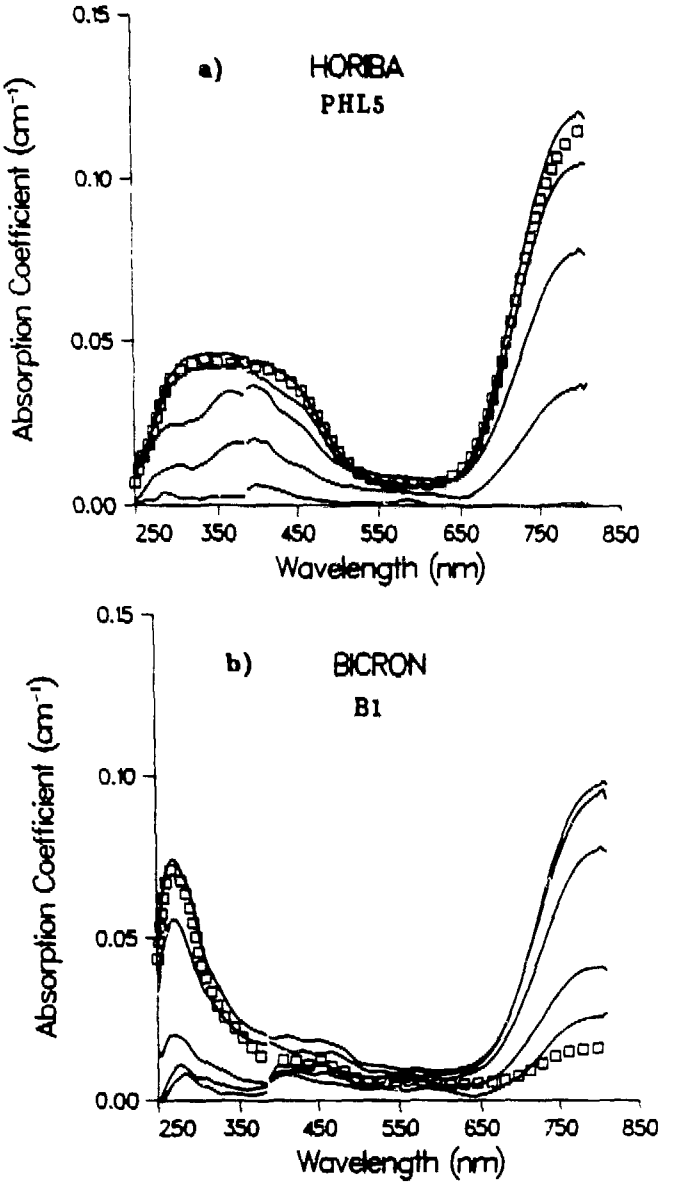

Fig. 11: Absorption coefficient vs. wavelength for various doses of ^{60}Co gamma radiation: 10^3, 10^4, 10^5, 10^6 and 1.5×10^6 rad a) Horiba b) Bicron. Squares show the recovery after 3 days in the dark at room temperature.

The relative intensity of the 250-550 nm bands differ appreciably between the two samples, as well as rate of growth of the different bands. In the Bicron crystal, the 800 nm band begins to saturate at higher doses, while in the Horiba crystal, the absorbance continues to grow. The opposite effect is true in the 250-500 nm region. In both cases, the absorption coefficient increased by $\sim$ .05 in the region of the fast scintillation emission, implying that the expected loss in light output due to increased absorption would be $\sim$ 12%. Both samples show little or no recovery in the short wavelength region, but the Bicron sample shows a substantial recovery for the 800 nm absorption band, where the Horiba sample shows almost

Table III

Change in Light Output and S/L Ratio After 1.5×10^6 Rad

Sample	Short gate	Long gate	S/L ratio
Horiba PHL3	-39%	-35%	-7%
Horiba PHL5	-10%	-15%	+8%
Horiba PHL7	-19%	-24%	+5%
Bicron B1	-29%	-36%	+9%
BDH A1	-26%	-27%	+1%

none. This could indicate different types or different amounts of impurities in the two crystals.

Table III give the percentage change in light output for the short and long gates and S/L ratio measured for the five samples after irradiation. It is again clear that there is a large sample to sample variation. The loss in light output varied from 10% for the best sample to ~ 40% for the worst. In most cases, this is considerably more than would be expected from the decrease in transmission, implying that there is an additional loss due to a reduction in the amount of light produced in the crystal. The S/L ratio changed by less than 10% in all cases, indicating that the damage affected the fast and slow components nearly equally. In all cases, the loss in light output is considerably less than would be expected in CsI(Tl) based on the results in ref. [14].

5. CONCLUSIONS

Several readout techniques for undoped CsI have been studied which utilise the fast component for use at high rates. Quantum yields have been measured for readouts using PMT's, wavelength shifters and silicon photodiodes. The PMT readout is best suited for measuring low energies with high resolution. The wavelength shifter readout gives a lower quantum yield but can be adapted to reading out large arrays with a limited number of PMT's. The silicon photodiode readout gives a high quantum yield, but due to the fact the diodes have no intrinsic gain, the energy resolution at low energies is dominated by the noise of the readout electronics.

The temperature dependence of the light output, decay time and emission spectrum of undoped CsI has been measured down to liquid nitrogen temperatures. It is found that the light output and decay time of the fast component increase substantially and the emission spectrum shifts to longer wavelengths at lower temperatures.

Radiation damage in undoped CsI has been measured for doses up to 1.5×10^6 rad of ^{60}Co gamma radiation. A reduction in light output is observed which is partly due to the formation of color center absorption bands in the wavelength region of the fast emission, and partly due to a reduction in light produced in the crystal. However, the total amount of damage observed is considerably less than has been reported in CsI(Tl).

ACKNOWLEDGMENT

We wish to thank E. Fernandes for his help in obtaining many of these results. This work was supported in part under Department of Energy Contract No. DE-AC02-CH7600016.

6. REFERENCES

1. S.Kubota et.al., Nucl. Inst. Meth. A268 (1988)275.
2. T.Towyama et.al., J. Phys. Soc. Japan 24 (1968)1133.
3. H.Kobayashi et.al., Kyoto University Preprint, KUNS-900, Nov. 1987.
4. The CLEO II detector, CLEO II Updated Proposal CLNS 85/634 (1985).
5. H.Kobayashi et.al., Kyoto University Preprint, KUNS-910, March 1988.
6. C.Woody, J. Tacetta and E. Fernandes, Technical Note 134, Brookhaven AGS Experiment 787, January 1989.
7. I.Holl et.al., IEEE Trans. Nucl. Sci. NS-35 (1988)105.
8. C.Bebek, Nucl. Inst. Meth. A265 (1988)258.
9. A.Zucchiatti et.al., Nucl. Inst. Meth. A281 (1989) 341.
10. P.Schotanus et.al., Nucl. Inst. Meth. A238 (1985)564;
    M. Suffert and G. Charpak, CERN EP/86-03, June 1986;
    K.Wisshak et.al., Nucl. Inst. Meth. A259 (1987)583;
    H. Kobayashi et.al., Kyoto University Preprint, KUNS-985, Oct. 1987.
11. D.F.Anderson, FERMILAB-Pub-89/169 (1989); to be published in Nucl. Inst. Meth..
12. Ya.A.Vablis, Z.A.Rachko and Ya.L.Yansons, JETP Lett. 42 (1985)172;
    S.Kubota et.al., Phys. Stat. Sol. B139 (1987)635.
13. R.V.Jones and J.H.Pollard, Proceedings of the Physical Society, Vol. 79, Part 2, No. 508 (1962).
14. M. Kobayashi and S.Sakuragi, Nucl. Inst. Meth. A254 (1987)275.
15. P.W.Levy, Society for the Advancement of Materials Process Engineering Journal, 21 (1985)35.
16. P.Avakian and A.Smakula, Phys. Rev. 120 (1960)2007;
    C.Bates, A.Salau and D.Leniart, Phys. Rev. B15 (1977)5963.

DISCLAIMER